ACS APPLIED MATERIALS & INTERFACES

www.acsami.org

Research Article

Hybrid Halloysite Nanotubes as Smart Carriers for Corrosion Protection

Adnan Khan, Amani Hassanein, Sehrish Habib, Muddasir Nawaz, R. A. Shakoor,* and Ramazan Kahraman

Cite This: *ACS Appl. Mater. Interfaces* 2020, 12, 37571−37584

Read Online

ACCESS | Metrics & More | Article Recommendations

ABSTRACT: Novel hybrid halloysite nanotubes (HHNTs) were developed and used as smart carriers for corrosion protection of steel. For this purpose, as-received halloysite nanotubes (HNTs) were loaded with a corrosion inhibitor, imidazole (IM), by vacuum encapsulation. In the next step, a layer by layer technique was employed to intercalate another inhibitor, dodecylamine (DDA), in the polyelectrolyte multilayers of polyethylenimine and sulfonated polyether ether ketone, leading to the formation of HHNTs. During this process, IM (5 wt %) was successfully encapsulated into the lumen of HNTs, while DDA (0.4 wt %) was effectively intercalated into the polyelectrolyte layers. Later, the HHNTs (3 wt %) were thoroughly dispersed into the epoxy matrix to develop smart hybrid self-healing polymeric coatings designated as hybrid coatings. For a precise evaluation, epoxy coatings containing as-received HNTs (3 wt %) without any loading denoted to as reference coatings and modified coatings containing HNTs loaded with IM-loaded HNTs (3 wt %) were also developed. A comparative analysis elucidates that the hybrid coatings demonstrate decent thermal stability, improved mechanical properties, and promising anticorrosion properties compared to the reference and modified coatings. The calculated corrosion inhibition efficiencies of the modified and hybrid coatings are 92 and 99.8%, respectively, when compared to the reference coatings. Noticeably, the superior anticorrosion properties of hybrid coatings can be attributed to the synergetic effect of both the inhibitors loaded into HHNTs and their efficient release in response to the localized pH change of the corrosive medium. Moreover, IM shows an active release in both acidic and basic media, which makes it suitable for the protection of steel at the early stages of damage, while DDA being efficiently released in the acidic medium may contribute to impeding the corrosion activity at the later stages of deterioration. The tempting properties of hybrid coatings demonstrate the beneficial role of the development of novel HHNTs and their use as smart carriers in the polymeric matrix for corrosion protection of steel.

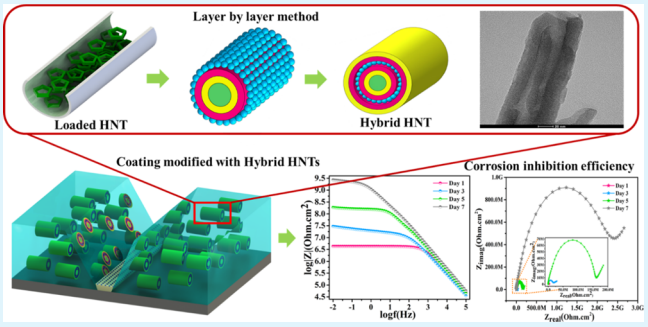

KEYWORDS: *hybrid halloysite nanotubes, imidazole, dodecylamine, smart coatings, corrosion inhibition*

1. INTRODUCTION

The global problem of corrosion is very challenging, and it is bothering the humankind for many centuries. Corrosion is considered as the most critical cause of material failure in all the industries where metallic parts are applied.[1−3] Organic coatings often are used to overcome corrosion challenges by limiting the contact of the metallic surfaces with an aggressive environment.[4] During the operation, the protective coatings may get damaged, which allows the aggressive media to penetrate the base metals and initiate corrosion.[5] Thus, self-healing smart coatings have been developed to overcome this problem[6−8] by reinforcing the polymeric matrices with nano/microcontainers loaded with active species of different functionalities.[9−11] These active species are sensitive to various stimuli and can be triggered by variation in temperature, pH, light, pressure or mechanical damage, and so forth.[12] Once released, these active species can hinder the attack of corrosive media and hence minimize the rate of corrosion.[13]

Recent literature is fertile with various active species encapsulated in inorganic particles such as cerium oxide,[14] zirconium oxide,[15] mesoporous silica,[16,17] halloysite nanotubes (HNTs),[18−21] titanium oxide,[22,23] calcium carbonate,[24] and so forth. The above-stated inorganic particles loaded with active species reinforced to polymeric matrices can self-heal the matrices by various mechanisms.[25] Hollow carriers are the most

Received: May 15, 2020
Accepted: July 20, 2020
Published: July 20, 2020

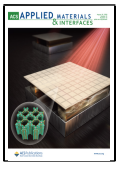

studied particles as these have the capability to store the active agents in the lumen of the carrier efficiently.[26,27] HNTs have hollow inner lumens in nanosize covered by the multiwalled aluminum silicate ($Al_2Si_2O_5(OH)_4 \cdot 2H_2O$). Unlike other tubular carriers, HNTs are natural, nontoxic, and environmentally friendly with great potential to store the active species for corrosion protection.[20,28,29] However, because of the firm van der Waals attractive forces in HNTs itself, it is difficult to ensure the uniform dispersion of these nanosize carriers in organic solvents.[26,30] Furthermore, the direct modification of the surface of HNTs is quite tricky because the majority of the hydroxyl groups reside on the inner surfaces of the tubes, and only a few are present on the outer surface.[31,32] One other major limitation is that these carriers hold individual active species, while the coating matrix requires simultaneously multiple active species to self-heal the damaged matrix.[33] Hence, it is preferable for the carriers to host multiples of the active agents in order to minimize the use of the carriers.[9,34]

In the present work, the concept of hybrid halloysite nanotubes (HHNTs) has been introduced to overcome the above-stated limitations. This is a novel strategy enabling different healing functionalities to reside on a single carrier, which can be reinforced into the epoxy matrix to develop innovative smart hybrid self-healing polymeric coatings. HHNTs were developed by loading the primary corrosion inhibitor, imidazole (IM), in the lumen of HNTs, while the secondary inhibitor dodecylamine (DDA) was intercalated into the polyelectrolyte multilayers of polyethylenimine (PEI) and sulfonated polyether ether ketone (SPEEK) formed on the surface of HNTs. The primary inhibitor was loaded into HNTs through the vacuum encapsulation process. In contrast, the secondary inhibitor (DDA) was intercalated into the multilayers using a layer by layer technique. As a next step, the synthesized HHNTs (3 wt %) were uniformly dispersed into the epoxy matrix to form smart hybrid self-healing polymeric coatings. For a clear comparison, the reference coatings, epoxy coatings composed of as-received HNTs without any loading, and modified coatings, the coatings formed by reinforcing the epoxy matrix with HNTs loaded with IM, were also developed. A comparison of the structural, thermal, mechanical, and anticorrosive properties of smart hybrid self-healing coatings is presented to elucidate the beneficial role of the development of HHNTs as new smart carriers. Our results confirm that the hybrid coatings demonstrate superior properties when compared to the reference coatings and modified coatings because of the synergetic effect of both the inhibitors loaded into HHNTs and their efficient release in response to the localized pH change of the corrosive medium. The tempting properties of hybrid coatings make them attractive for corrosion protection of steel.

2. EXPERIMENTAL SECTION

2.1. Materials and Chemicals. The HNTs ($Al_2Si_2O_5(OH)_4 \cdot 2H_2O$), used as a substrate for the deposition of polyelectrolyte multilayers, were purchased from Sigma-Aldrich, Darmstadt, Germany. IM-a primary inhibitor, DDA-secondary inhibitor, PEI, SPEEK, ethanol, and sodium chloride were also provided by Sigma-Aldrich and used without further purification. Epoxy resin (EPON RESIN 815C) and its curing agent (EPIKURE) was purchased from Hexion chemicals, and dimethylacetamide was supplied by BDH chemicals Ltd. Carbon steel sheets used as a substrate for coatings were purchased from a local source. The steel substrates were ground using silicon carbide (SiC) abrasive papers supplied by Hasuco Korea. The substrates were thoroughly rinsed with water and cleaned with ethanol before applying coatings.

2.2. Loading of IM into HNTs. The primary inhibitor (IM) was encapsulated into the HNTs through a vacuum method, as reported in the previous reports.[35,36] During this procedure, 2 g of HNTs was added to 40 mL aqueous solution of IM (80 mg mL^{-1}). The suspension of HNTs and IM was sonicated for 30 min to ensure proper dispersion of HNTs in the solution. The suspension was then transferred to the vacuum chamber connected with a rotary pump. The vacuum process was conducted for eight hours to remove the air from the lumen of HNTs and to load IM inside the lumen of the HNTs. After performing the vacuum treatment, the suspension was returned to atmospheric pressure. The vacuum cycling treatment was repeated three times (1 h each) to ensure efficient loading. Finally, to remove the excess of water, the samples were centrifuged, rinsed with water, and dried for 5 h at 70 °C. The dried powder of loaded HNTs was then collected and saved for further characterization and coating. A schematic diagram showing the loading of IM into HNTs is presented in Figure 1.

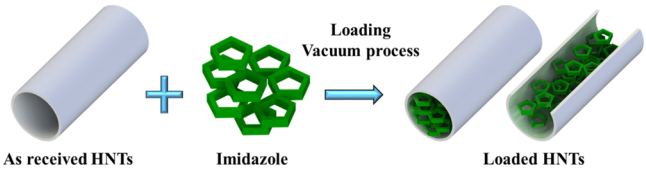

Figure 1. Schematic representation of loading IM into the as-received HNTs.

2.3. Synthesis of Hybrid HNTs by the LBL Technique. Unlike other nanotube structures (carbon nanotubes, titanium nanotubes, etc.), HNTs have a distant inner lumen and outer surface chemistry, allowing active species of various functionalities to modify them. The lumen of HNTs is positively charged because of $Al(OH)_3$, while the outer surface has a negative charge because of the presence of SiO_2. Making use of this morphological behavior of HNTs, a layer by layer technique was used to intercalate a secondary corrosion inhibitor (DDA) into the polyelectrolyte layers deposited on the surface of HNTs loaded with IM as presented in the schematic diagram (Figure 2a). The positively charged PEI was first deposited on the surface of loaded HNTs (HNTs + IM) by mixing 2.0 mg of mL^{-1} solution of PEI (60.0 mL) with 40 mL of suspension of HNTs for 10 min at 300 rpm. The negatively charged SiO_2 on the outer surface of HNTs binds with positively charged PEI. The excess of water and PEI from the developed (HNTs + IM)/PEI was removed by centrifuging, followed by rinsing with ethanol and water. The second layer of negative polyelectrolyte SPEEK was adsorbed on (HNTs + IM)/PEI by mixing 40 mL of suspension of (HNTs + IM)/PEI for 10 min at 300 rpm with the 60 mL of solution of SPEEK (2 mg mL^{-1} in dimethylacetamide) to synthesize (HNTs + IM)/PEI/SPEEK. The excess of SPEEK was removed in a similar fashion as used in the first layer. The third layer deposited was of DDA, which was positively charged, and was used as a secondary inhibitor in HHNT design. Suspension (40 mL) of the resulted (HNTs + IM)/PEI/SPEEK was mixed with 60 mL of solution of DDA (10 mg mL^{-1}) for 20 min at 300 rpm while maintaining the pH at 3 during this layer deposition process. The fourth and fifth layers of SPEEK and PEI were deposited following the previous procedure to develop final HHNTs ((HNTs + IM)/PEI/SPEEK/DDA/SPEEK/PEI). Figure 2b,c represents loading of inhibitor (IM) into HNTs and the electrostatic attraction between the consecutive layers of HHNTs.

2.4. Preparation of Coatings. Three different types of epoxy coatings were developed; (i) reference coatings, the epoxy coatings composed of as-received HNTs without any loading, (ii) modified coatings, the coatings formed by reinforcing epoxy matrix with loaded HNTs, and (iii) smart hybrid self-healing polymeric coatings developed by incorporating HHNTs into the epoxy matrix. All the above prepared coatings were applied to the steel substrates using the doctor blade technique.

Carbon steel plates ($30 \times 30 \times 1$ mm^3) were used as substrates. The substrates were ground with silicon carbide abrasive papers, washed with water and ethanol, and dried with a hot air gun before the

https://dx.doi.org/10.1021/acsami.0c08953
ACS Appl. Mater. Interfaces 2020, 12, 37571−37584

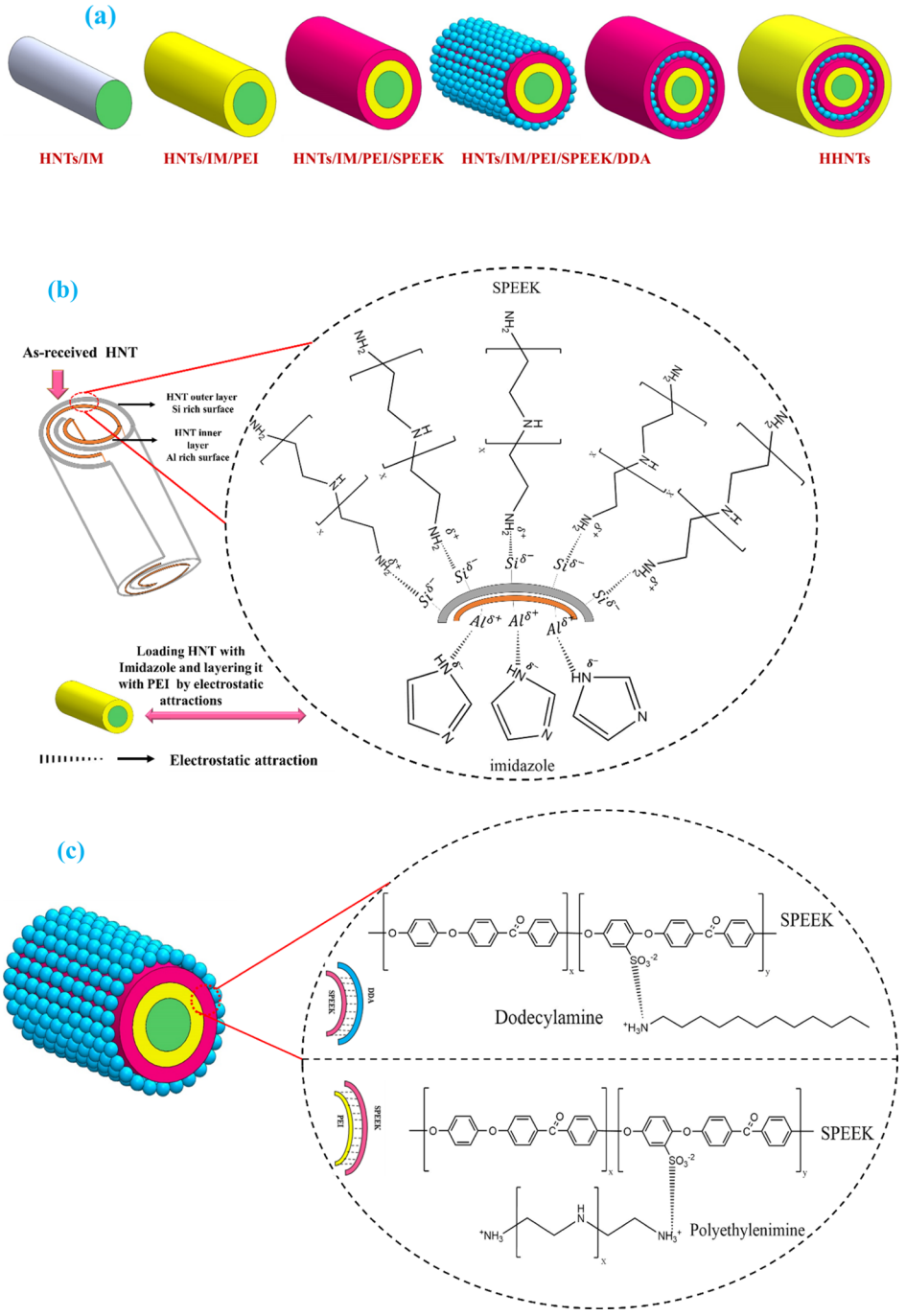

Figure 2. Schematic representation; (a) synthesis of HHNTs and (b,c) loading of HNTs and the electrostatic attraction between the consecutive layers of HHNTs.

commencement of the coating process. A model epoxy (EPON 815C) was used as a coating material. The samples were coated by mixing epoxy with the hardener (EPIKURE curing argent 3282) (5:1). A predetermined amount (3 wt %) of reinforcement (as-received HNTs, loaded HNTs, and HHNTs) was mixed with the hardener and then added to the epoxy resin to develop, (i) reference coatings, (ii) modified coatings, and (iii) hybrid coatings. The epoxy mixtures were kept for 10 min sonication followed by 10 min vacuum to achieve a well-dispersed and bubble-free epoxy mixture. The epoxy mixture was applied on the steel substrates with the doctor blade to obtain a uniform thickness of ∼200 μm. The prepared coatings were cured for 48 h at room temperature to attain a dry film. A manual scratch of ∼180 μm width was made using a scalpel on the coatings before the electrochemical impedance evaluation. The scratch will allow the coatings to start the spot corrosion, which will increase to localize pH, which in turn will trigger to release the loaded inhibitors.

2.5. Characterization of the Nanotubes and the Developed Coatings. The Fourier transform infrared (FTIR) study (FTIR Frontier, PerkinElmer, Frontier, USA) was carried out to confirm the loading of IM in the HNTs and to verify the successful formation of HHNTs. The spectra were recorded in the range of 500−4000 cm^{-1} in a transmission mode. The morphology of as-received HNTs, loaded HNTs, and HHNTs was analyzed by field emission scanning electron microscopy (FE-SEM-Nova Nano-450, Netherland) and transmission electron microscopy (TEM) coupled with high-resolution energy dispersive X-ray spectroscopy (EDS) (TEM, FEI, TALOS F200X, USA). To quantify the loading of inhibitors and to calculate the specific surface area (SSA) and pore volume (PV) of as-received HNTs, loaded

https://dx.doi.org/10.1021/acsami.0c08953
ACS Appl. Mater. Interfaces 2020, 12, 37571−37584

HNTs, and HHNTs, the Brunauer−Emmett−Teller (BET) technique was used (surface area analyzer, Micromeritics ASAP 2420, USA). Zeta potential equipment (Malvern, Zeta sizer, Nano ZSP, USA) was employed to analyze the surface charges on the individual layer of the HHNTs during the layer by layer technique. X-ray photoelectron spectroscopy (XPS) (AXIS Ultra DLD, Kratos, UK) using a monochromatic X-ray source—Al Kα source was used to ensure the surface chemical composition and adsorption of the multilayers with an intercalated inhibitor on the surface of HHNTs. The binding energy of C 1s (284.6 eV) was used as a reference. The energy resolution was 160 eV, and the spatial resolution was 20 eV. Thermal stabilities of the as-received HNTs, loaded HNTs, HHNTs, and the prepared coatings were studied between the temperature range of 40 to 600 °C employing a heating rate of 20 °C/min. Thermal gravimetric analysis (TGA) and differential thermal gravimetric analysis (DTA) profiles were obtained by a synchronization analyzer (PerkinElmer, TGA 4000, USA). UV−vis spectroscopic analysis (LAMBDA 650 UV−vis Spectrophotometer, PerkinElmer, USA) was employed to analyze the release of inhibitors from the loaded HNTs and HHNTs. Various solutions with different pH values were prepared, and small amounts (0.1 g) of loaded HNTs and HHNTs were added to determine the release behavior of loaded inhibitors at different pHs and after different immersion times. An analytical balance with density determination equipment (Sartorius YDK03) was used for porosity measurements. The Vickers Microhardness tester (MKV-h21, Japan) was used to determine the hardness of the developed coatings. All measurements were performed under a load of 50 gf for 10 s. Universal testing machine (Lloyd-Ametek LR50K Plus, USA) was employed to study the tensile behavior of the developed coatings. Tensile testing of the developed coatings was performed at room temperature, applying an engineering strain rate of 10^{-4}/s under uniaxial tensile loadings.

Electrochemical impedance spectroscopy (EIS) tests were performed to evaluate the corrosion impeding capability of the developed coatings in 3.5 wt % of NaCl solution at room temperature. The EIS spectra were recorded in the frequency range of 10 mHz to 100 kHz using Gamry 3000 equipment (30K BOOSTER potentiostat/galvanostat/ZRA, USA). A three-electrode system was used in which the coated steel plates were used as working electrodes, with an exposed area of 0.5 cm^2, and a platinum wire was used as a counter electrode while an Ag/AgCl electrode was employed as a reference electrode. A controlled defect of 5 cm length was made manually on the developed coatings to study their inhibition effect. The coated samples were exposed to a 3.5% NaCl solution, and the electrochemical tests were performed at an exposure time of 1, 3, 5, and 7 days. The EIS tests were repeated three times to ensure reproducibility.

3. RESULTS AND DISCUSSION

3.1. FTIR Spectroscopy. Figure 3 depicts the FTIR spectra of as-received HNTs, loaded HNTs, and HHNTs. In the as-received HNTs (Figure 3a), the absorption bands at 3697, 3625, and 1648 cm^{-1} show the stretching of Al−OH bond and OH deformation of water in HNTs.[37] Furthermore, the characteristic peaks at 1116 and 1004 cm^{-1} belong to the perpendicular and in plan Si−O bond because of the majority of O−S−O groups on the surface of HNTs. In addition, the absorption peaks present at 905 and 538 cm^{-1} correspond to the bending vibration of Al−OH and the deformation of the Al−O−Si group.[38] A comparison of the FTIR spectrum of loaded HNTs (Figure 3c) and as-received HNTs (Figure 3a) indicates the presence of some additional peaks. These new peaks at 3118, 3025, and 2914 cm^{-1} can be ascribed to the C−H stretching, while the absorption peak at 1326 and 1188 cm^{-1} belongs to the aromatic amine group of IM.[39] The formation of these new peaks in the IR spectrum verifies the successful loading of HNTs with IM.

In the IR spectrum of HHNTs (Figure 3e), the absorption peaks at 3697, 3625, 1648, 1116, and 1004 cm^{-1} are consistent

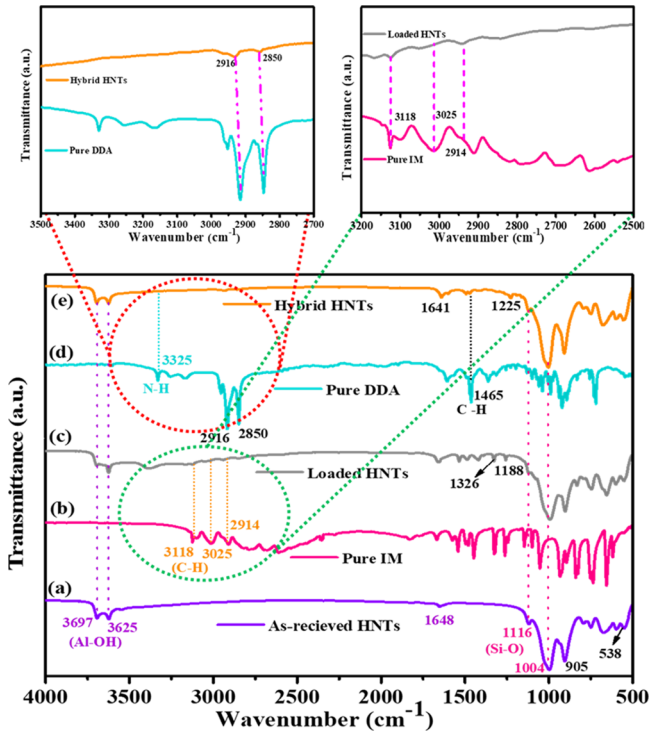

Figure 3. FTIR spectra; (a) as-received HNTs, (b,c) pure IM and loaded HNTs, and (d,e) pure DDA and hybrid HNTs.

with the IR spectrum of as-received HNTs and loaded HNTs which is originated from HNTs. The small absorption peak at 3325 cm^{-1} corresponds to the amine group of DDA, which is used as a secondary corrosion inhibitor.[40] The partial absorption peak of N−H in the spectrum HHNTs could not be discriminated because of the broad and robust peak of pure DDA. The new characteristic peak at 1641 and 1225 cm^{-1} in the IR spectrum of HHNTs represents C═C and C−N stretching, respectively, which can be ascribed to DDA, PEI, and SPEEK.[8] In addition, the peak adsorption at 1465 cm^{-1} represents the C−H stretching of HHNTs. A close comparison of the IR spectra of as-received HNTs, loaded HNTs, and HHNTs verifies the formation of polyelectrolyte multilayers on the surface of HNTs and the intercalation inhibitors (DDA and IM) without any side reactions.

3.2. SEM Analysis. Figure 4 depicts the morphological study of the as-received HNTs and loaded HNTs observed by FE-SEM. The FE-SEM analysis of as-received HNTs (Figure 4a,b) revealed a tubular structure without any clusters. The sample results also explained various sized tubular morphology of nanotubes. The cluster free nanotubes reflect the dry surface of as-received HNTs. On the other hand, the FE-SEM of loaded HNTs (Figure 4c,d) also revealed a similar morphology as the received HNTs with a few clusters in the sample. The presence of clusters in the loaded HNTs maybe because of the sticky surface of the loaded HNTs after loading with a negatively charged inhibitor. The results are in line with the already reported literature.[41]

3.3. TEM Analysis. In order to confirm the adsorption of polyelectrolyte layers on the surface of loaded HNTs, TEM and high-resolution EDS elemental mapping were carried out. Figure 5a−c shows the TEM images of the HHNTs. The dark inner space of loaded HNTs confirms the efficient loading of IM, while the smooth deposited surfaces indicate the adsorption of

https://dx.doi.org/10.1021/acsami.0c08953
ACS Appl. Mater. Interfaces 2020, 12, 37571−37584

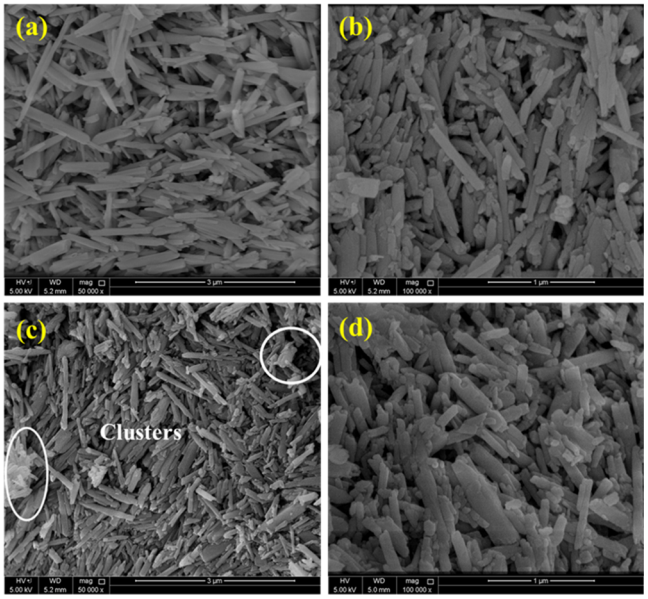

Figure 4. FE-SEM images of HNTs (a,b) as-received HNTs and (c,d) loaded HNTs.

polyelectrolytes on the surface of HNTs.[42] Furthermore, the high amount of oxygen and the presence of carbon and nitrogen in the EDS analysis (Figure 5d−h) also confirm the deposition of organic species on the surface of HHNTs. Figure 5g is the carbon mapping which depicts both the content of carbon on the grit and in the particles itself. The presence of carbon in the particle verifies the carbon-based deposition on HNTs. The morphological observation of the HHNTs is in good agreement with the FTIR analysis, indicating that the polyelectrolyte multilayers, along with the sandwiched DDA, are successfully assembled. These findings are consistent with previous studies.[42]

3.4. BET Surface Area and PV of as-Received and Hybrid HNTs. To quantify the loading efficiency, BET SSA and PV of as-received HNTs, loaded HNTs, and HHNTs were measured. Figure 6 presents the N_2 adsorption−desorption isotherms of the samples, which has relatively a different pressure type H3 hysteric loop. These types of hysteresis loop

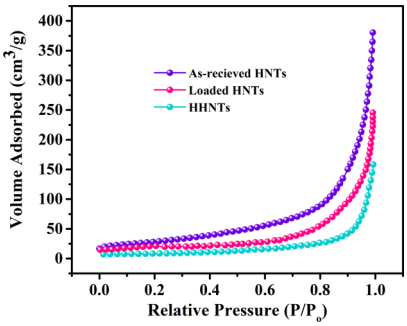

Figure 6. Nitrogen adsorption−desorption isotherms of the as-received HNTs, loaded HNTs, and hybrid HNTs samples.

usually describe the mesoporous and macropores structures. By calculating the SSA and PV of loaded HNTs, there was a substantial decrease compare to as-received HNTs.[43,44] The SSA and PV decreased from 102.7 m^2/g and 0.591 cm^3/g to 56.2 m^2/g and 0.351 cm^3/g, respectively. A ∼46% decrease in SSA and ∼41% decrease in PV was observed after loading IM in HNTs (Table 1). This substantial decrease in SSA and PV

Table 1. BET Surface Area and BET Pore Volume of as-Received HNTs, Loaded HNTs, and Hybrid HNTs

sample	BET specific surface area (m^2/g)	BET pore volume (cm^3/g)
as-received HNTs	102.7	0.591
loaded HNTs	56.2	0.351
HHNTs	25.6	0.246

confirms the efficient loading of IM within the lumen of HNTs. The SSA and PV were further decreased by ∼54 and ∼32%, respectively, in HHNTs, which verify the adsorption of compact and pore-free polyelectrolyte layers on the surface of HNTs.

3.5. Zeta Potential Analysis. HNTs have typically an alumosilicate multiwall tubular structure in which the majority of silica lies on the outer surface of the HNTs. Hence, the electrical ζ potential on its surrounding surface is negative (∼−30 mV) because of the negatively charged silica. This ζ potential is much smaller than the pure silica ζ potentials (∼−50 mV) because of the superposition of positively charged

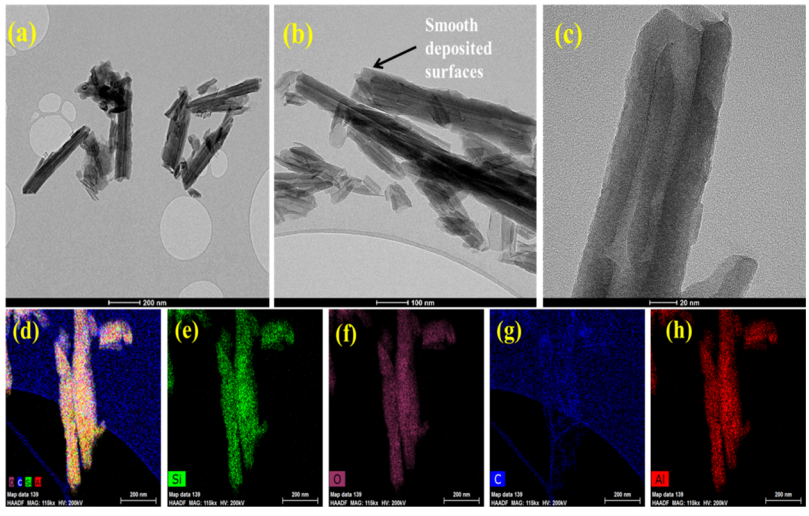

Figure 5. (a−c) TEM images of HHNTs at different resolution and (d−h) high-resolution EDS of the HHNT sample.

https://dx.doi.org/10.1021/acsami.0c08953
ACS Appl. Mater. Interfaces 2020, 12, 37571−37584

$Al(OH)_3$ in the lumen.[45] The negative surface potential allows HNTs to modify its surface with positive materials. Hence, zeta potential analysis was carried out to ensure the adsorption of each layer on the surface of HNTs represented in Figure 7. It was

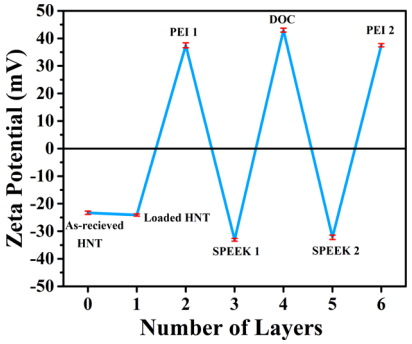

Figure 7. Zeta potential charge on as-received HNTs, loaded HNTs, and different layers of HHNTs.

noticed that the ζ potential of the as-received HNTs and HNTs loaded with MI is negative as expected. The negative ζ potential of loaded HNTs confirms the presence IM only in the lumen of HNTs. After the deposition of polycation PEI, the ζ potentials are shifted to a positive value of 45 mV. Furthermore, after the adsorption of SPEEK, the ζ potential is moved to negative value because of the $-SO_3$ group in SPEEK. The sulfonic group of SPEEK is also responsible for binding the amine groups of PEI and DDA with SPEEK. Therefore, the zeta potential is also dramatically shifted to the positive value (~33.2 mV) after the deposition of the DDA layer. The change in the ζ potentials after the deposition of each layer is evidence of the successful adsorption of the polyelectrolyte layers on the surface of HNTs. Variation of ζ potentials with polyelectrolyte layers has also been reported in the previous studies.[45−47]

3.6. XPS Analysis. The XPS analysis was carried out to study the detailed surface elemental composition of the loaded HNTs and HHNTs. Figure 8a−c presents the XPS spectrum of aluminum, silicon, and oxygen, which are detected as major elements on the surface of loaded HNTs. The Si/Al ratio of 1.14 (Table 2) is observed because of the majority of silica present in

Table 2. XPS Surface Elemental Compositions of Loaded HNTs and HHNTs

	surface chemical composition, atomic %				
sample	Al	Si	O	C	N
loaded HNTs	12.78	14.57	72.64		
HHNTs				89.33	10.67

the outer surface of loaded HNTs. The absence of carbon and nitrogen in the surface composition of loaded HNTs confirms the successful loading of IM in the lumen of as-received HNTs.[48] A relatively large amount of oxygen is detected on the surface loaded HNTs, which represents the typical HNTs structure having the majority of oxygen both on the outer and inner layer of the helical multilayers of aluminosilicate. Furthermore, the fitting peak of aluminum in the XPS spectrum of loaded HNTs at 74.6 eV represents the presence of aluminum oxide. The silicon spectrum shows only the bonding energy of SiO_2 at 103.4 eV. On the other hand, the oxygen spectrum depicts the fitting peaks at 531.2 and 532.8 eV, which is representing the bonding energy of Al_2O_3 and SiO_2 on the surface of loaded HNTs.[49]

On the contrary, carbon and nitrogen are the elements detected in the surface HHNTs presented in Figure 8d,e. The C 1s spectrum of the HHNTs shows the fitting peaks at 284.6, 286.3, and 288.3 eV, representing the bonding energy of C−C bond C−O bond and C═O bond, respectively. The $C-NH_2$ bonding energy also confirms from the XPS spectrum of nitrogen in the HHNT surface. The carbon and nitrogen bonding energies reflect the structures of PEI and SPEEK used as outer layers in HHNTs. The XPS analysis confirms the successful loading of IM into HNTs and adsorption of the polyelectrolyte multilayers on the surface of HNTs without any impurities.

3.7. Thermal Stability of HNTs and Modified Coatings. Figure 9a,b depicts the TGA and DTA of as-received HNTs, loaded HNTs, and HHNTs. According to the inset Figure 9a, both the organic inhibitors (DDA and IM) have a complete decomposition at 198 and 230 °C, respectively. The TGA/DTG curve of loaded HNTs shows a first weight loss peak at 246 °C, which corresponds to the decomposition of the loaded IM in

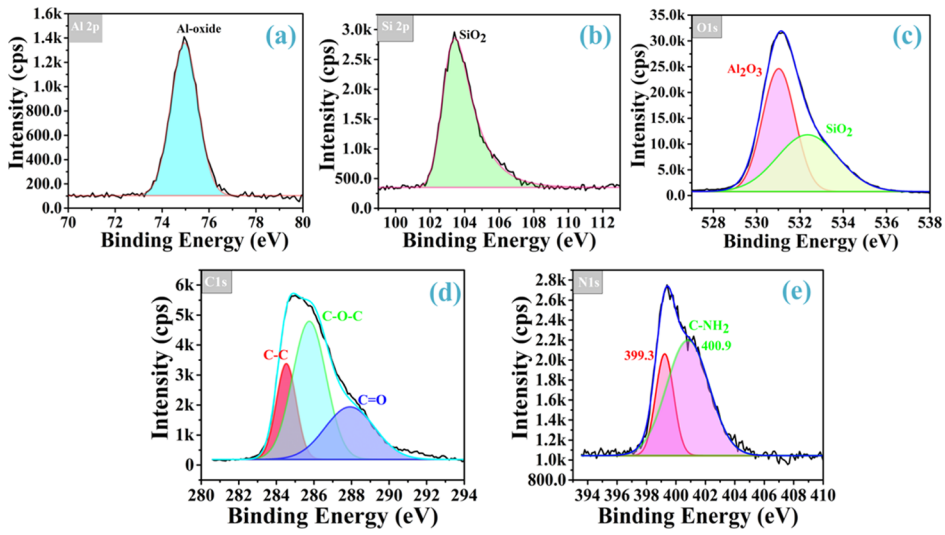

Figure 8. XPS spectra presenting the surface elemental composition; (a−c) loaded HNTs and (d,e) HHNTs.

https://dx.doi.org/10.1021/acsami.0c08953
ACS Appl. Mater. Interfaces 2020, 12, 37571−37584

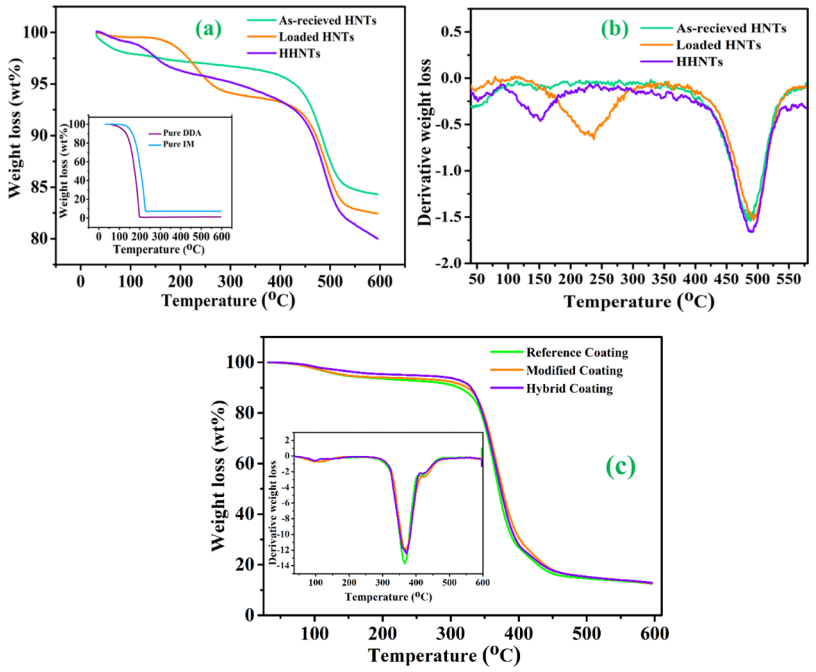

Figure 9. Thermal analysis; (a,b) TGA results and DTA curves of the as-received HNTs, loaded HNTs, and HHNTs (c) TGA and DTA curves of the reference coatings, modified coatings, and smart hybrid self-healing polymeric coatings.

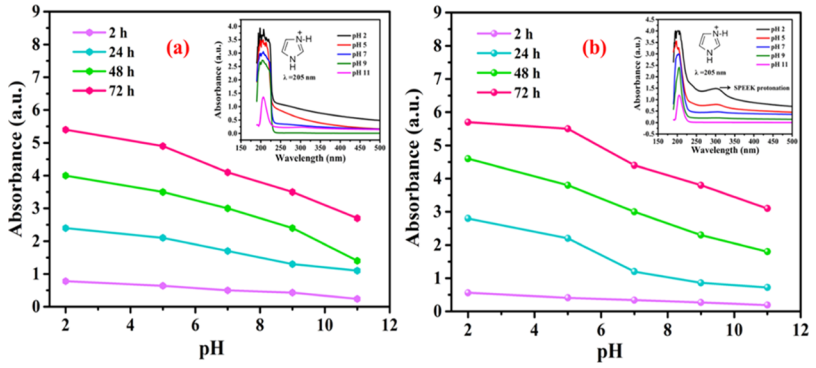

Figure 10. UV−vis spectroscopy (a) release behavior of IM from loaded HNTs immersed in different pH solutions for 2, 24, 48, and 72 h. (b) Release behavior of IM from HHNTs, the inset is the spectra of HHNTs immersed in various pH solutions after 48 h.

HNTs. Furthermore, there is a shift in the derivative weight loss peak of loaded HNTs, which can be ascribed to the physical interaction of IM with the lumen of HNTs, resulting in its higher stability. The second weight loss peak of loaded HNTs is observed at 488 °C, which is due to the decomposition of HNTs.[50] Considering the initial minor weight loss peaks, which can be due to entrapped water content in the multi walls of HNTs, it can be concluded that 5 wt % of IM is loaded into HNTs. By analyzing the TGA/DTA curve of HHNTs, five possible slopes (inflection points) are identified, which will be related to different weight loss. In order to measure the loading efficiency of DDA in the polyelectrolyte layers, it is essential to stress the comparison of both loaded and HHNTs curves. Because in both samples, the base material (clay) is the same, therefore, any additional peak in the curve will correspond to the loaded organic inhibitors (IM and DDA) or the polyelectrolyte shells. In the case of HHNT slopes from 40 to 170 °C, it can be assigned that the weight loss of absorbed and structural water is almost 3.8 wt %. The slop in the range of 210−470 °C, which sums the weight loss of 5.4 wt %, is corresponding to the complete decomposition of the organic (IM and DDA) in the lumen and external shells.[51] Therefore, the loading efficiency of the intercalated DDA can be estimated as 0.4 wt %. The slope from 470 to 530 °C shows the dihydroxylation of the halloysite clay, which sums the weight loss of 6.4 wt %. The last steeper slope in the range of 540−600 °C can be attributed to the highly stable polyelectrolyte molecules.

Moreover, Figure 9c presents the TGA and DTA of the reference coatings, modified coatings, and hybrid smart coatings. All developed coatings show an identical highest peak of thermal degradation at 380 °C, which can be attributed to the thermally stable epoxy monomer and the doped HNT-based nanoparticles. The TGA and DTA curves confirm that the prepared coatings are thermally stable up to 380 °C, which is quite decent considering their end-users, that is, the oil and gas industry. These findings are also consistent with the previous studies.[52,53]

3.8. UV−vis Spectroscopic Analysis. Self-release of corrosion inhibitor from loaded HNTs and HHNTs was studied through UV−vis spectroscopy. The loaded HNTs and HHNTs were separately dispersed into 0.1 M NaCl solution having different pH values (2, 5, 7, 9, and 11). The UV spectra of both

https://dx.doi.org/10.1021/acsami.0c08953
ACS Appl. Mater. Interfaces 2020, 12, 37571−37584

loaded HNTs and HHNTs were studied as a function of pH after 2, 24, 48, and 72 h, as shown in Figure 10a,b. In the case of loaded HNTs (Figure 10a), it can be noticed that the profiles of spectra obtain at different pHs are identical in nature. In the case of loaded HNTs, a clear peak is observed at 205 nm, which corresponds to the aromatic structure of IM.[54,55] The loaded HNTs showed the absorbance in all acidic, neutral, and basic media (Figure 10a). The highest absorbance intensity was observed at pH 2, which decreases with increasing pH of the solution. This result suggests that the self-release of IM is sensitive to the pH of the solution. The efficient release of IM is observed in an acidic medium instead of a basic medium, although the self-release of IM is noticed at all pH values.

On the other hand, two distinct peaks of intensities (205 and 310 nm) were noticed in HHNTs presented in Figure 10b. The 205 nm is the lambda max of IM, which clearly showed the release of IM with different pHs from the lumen of hybrid HNTs.[54] The 310 nm peak corresponds to the protonation of SPEEK, which has a conjugated structure used as a polyelectrolyte layer.[56] From the dominant peak (310 nm) at lower pH, it can be realized that the polyelectrolyte SPEEK layer can be easily protonated in acidic medium and can release the intercalated DDA. It can be concluded that in acidic medium, both IM and DDA show an efficient self-release enabling corrosion protection at the later stages of corrosion damage, whereas in neutral and basic medium, only IM shows promising self-release, which makes IM efficient at the early stage of corrosion protection. Furthermore, from the 310 nm peak, a successful polyelectrolyte multilayer formation on the surface of HNTs can also be confirmed.

3.9. Mechanical Properties of the Prepared Coatings. HNTs consist of silica-based exterior surface and aluminum on their interior surface, which are both polar, and enable them to be well dispersed in polar polymers such as epoxy. The high strength (130 GPa) and high flexibility (ability to bend 90° without failure) of HNTs make them a suitable reinforcement for the epoxy matrix to improve the tensile strength of polymeric coatings. The mechanical properties of pure epoxy, reference coatings, modified coatings, and hybrid coatings are summarized in Table 3. It is evident that the density of coatings increased by

Table 3. Mechanical Properties of Pure Epoxy, Reference, Modified, and Hybrid Coatings

samples	density (g/cm^3)	Vickers hardness	tensile strength (MPa)
pure epoxy	1.67	18 ± 2	0.8 ± 0.1
reference coating	1.78	33 ± 3	1.5 ± 0.2
modified coating	1.80	34 ± 2	1.54 ± 0.2
hybrid coatings	1.84	37 ± 4	1.65 ± 0.3

the addition of HNTs. Hybrid coatings show the highest increase in the density because of the loading of inhibitors and the presence of multilayers on the surface of HNTs. Furthermore, the Vickers hardness of reference coatings increased with the incorporation of HNTs into the epoxy matrix. Hybrid coatings demonstrate the highest improvement in the hardness (~105%) as compared to the reference coatings. A similar trend is noticed in the tensile strength reaching its maximum value (1.65 ± 0.3) in smart hybrid self-healing polymeric coatings. The calculated increase in the tensile strength is ~106% as compared to the reference coatings. The significant enhancement in the mechanical properties of the hybrid coatings can be attributed to the (i) dispersion hardening effect due to the presence of insoluble and hard ceramic HNTs, (ii) formation of a composite structure which improves the load bearing properties, and (iii) the enrichment of the dislocation density. These findings are consistent with the previous studies.[42,57]

Moreover, the increase in mechanical properties of the developed coatings is attributed to the uniform dispersion of HNTs in the epoxy matrix and their strong tubular interfacial interactions.[58] The well-dispersed HNTs causes crystallization of epoxy monomers, providing significant improvement in mechanical properties.[20] The nanoclay provides a ceramic skeleton within the polymeric matrix, enhancing the strength.[59] Also, halloysite nanoclay has better compatibility with epoxy; the strong tubular interaction of HNTs with epoxy provides strong adhesion and hence improves the mechanical properties of these coatings.[60]

3.10. Electrochemical Evaluation of the Prepared Coatings. The electrochemical performance of reference coatings, modified coatings, and hybrid coatings was analyzed in 3.5 wt % NaCl solution for seven days after providing controlled damage on their surface. Figure 11 represents the

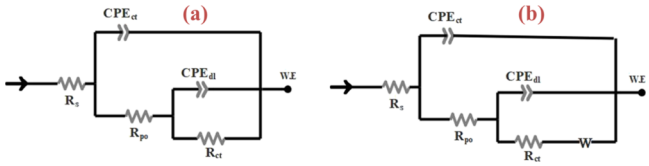

Figure 11. Equivalent circuits used for EIS analysis of (a) reference coating and (b) modified and hybrid coatings.

equivalent circuits used to fit the experimental data in order to quantify the essential electrochemical parameters. The EIS spectra of the reference coatings were fitted by a two-time constant circuit (Figure 11a), whereas two-time constant circuit with a Warburg diffusion coefficient (W) was used to fit the EIS results of modified and hybrid coatings, as shown in Figure 11b. These equivalent circuits quantify the parameters of the electrochemical reactions occurring on the surface of the scratched coated samples.[61,62] The key electrochemical parameters include the solution resistance (R_s), pore resistance (R_p), charge transfer resistance (R_{ct}), and capacitance of the coatings (CPE), that is, double-layer capacitance and coating capacitance. R_s is solution resistance offered by the electrolyte solution, R_p is the resistance provided by the scratch-made in the coating, and R_{ct} is the resistance provided by the applied coatings. The R_p and CPE of the coatings were evaluated by the high-frequency time constant, while the R_{ct} and double layer capacitance were extracted by the low-frequency time constant.

Figure 12 depicts the characteristic impedance spectra of the reference and modified coatings. The reference coatings show an impedance modulus of about 7.5×10^6 Ω. This decent resistance can be attributed to the doped HNTs in the epoxy matrix. The impedance value shows a decreasing trend with increasing immersion time and reaches to 5.62×10^5 Ω after the seventh day. This reduction of the impedance value is due to the uptake of the electrolyte by the scratched area of the coatings, which provides a conductive path to the corrosive medium. As a consequence, the impedance value shows one order of decrease in its value as compared to the initial stage of immersion. When the electrolyte species reach the steel substrate, spot corrosion initiates as confirmed by the decay in the low frequency bode

https://dx.doi.org/10.1021/acsami.0c08953
ACS Appl. Mater. Interfaces 2020, 12, 37571−37584

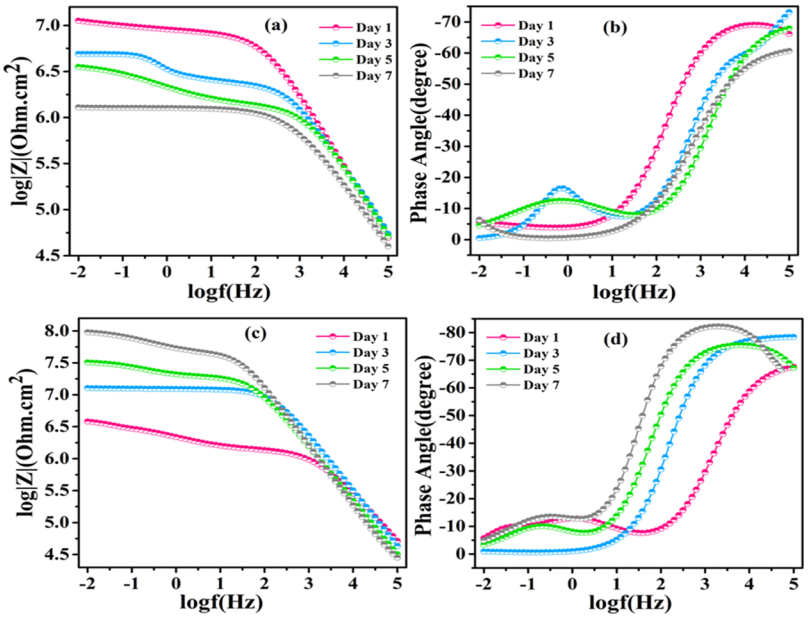

Figure 12. EIS bode spectra and phase angle of coatings after immersion in 3.5 wt % of NaCl solution for different time intervals; (a,b) reference coating (c,d) modified coatings.

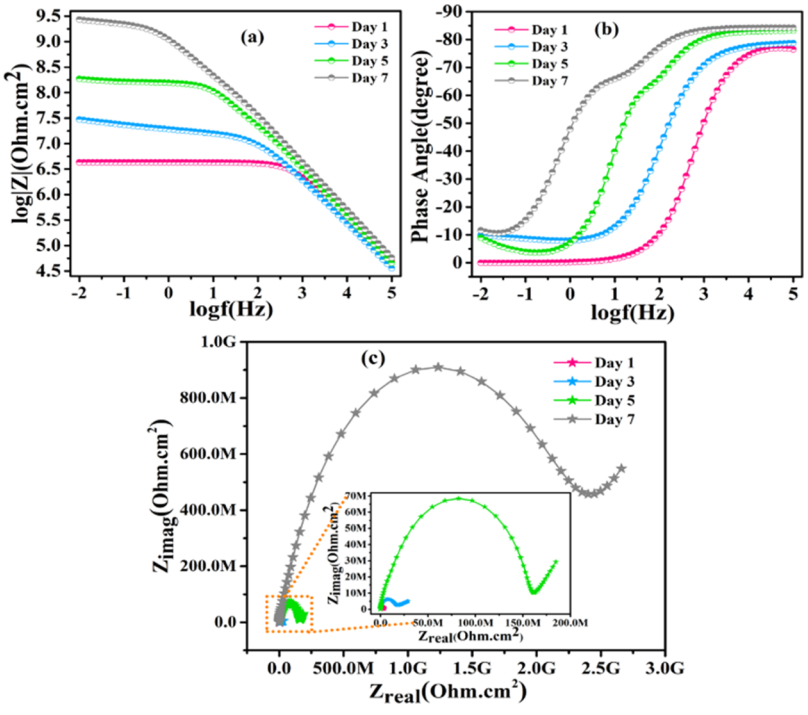

Figure 13. EIS results of the hybrid coatings after immersion in 3.5 wt % solution; (a) bode spectra, (b) phase angle and (c) Nyquist plot.

and phase angle spectra (Figure 13a,b). On the other hand, the modified coatings (Figure 12c,d) show different behaviors at various stages of immersion. The impedance value shows a continuous increase in its value with the increase in the immersion time, which verifies the inhibition efficiency of the IM in the scratched coatings. The highest impedance of 4.1×10^7 Ω is observed after the seventh day of immersion, which is increased by one order compared to the reference coatings. At low-frequency range (of bode and phase angle), the value of impedance and phase angle increases with immersion time, showing an incremental increase in the barrier properties of the modified coatings. The gradual increase in the impedance values of modified coatings with increasing immersion time reflects their decent barrier properties against corrosion by providing additional inhibitive protection. The inhibition efficiency percentage (IE %) of the modified coatings with respect to the reference coatings can be calculated using the following equation.[22]

$$\text{IE \%} = \frac{(R_{ct},\ \text{modified} - R_{ct},\ \text{reference})}{(R_{ct},\ \text{modified})} \times 100 \quad (1)$$

https://dx.doi.org/10.1021/acsami.0c08953
ACS Appl. Mater. Interfaces 2020, 12, 37571−37584

The highest calculated inhibition efficiency of modified coatings is ~92% after the seventh day of immersion when compared to the reference coatings.

Figure 13 shows the EIS spectra of the hybrid coatings. The scratched hybrid coatings reveal almost similar impedance as the modified coatings at the initial stage of immersion. Over the immersion time, the hybrid coatings show a gradual increase in the impedance value with increasing immersion time, reflecting the synergetic barrier properties two loaded corrosion inhibitors (IM and DDA). The maximum impedance value after the seventh day of the immersion time is ~2.01×10^9 Ω, which is two orders higher when compared to the modified coatings and three orders higher when compared to the reference coatings. At lower frequency range, an increment in the impedance value is accompanied by the shift in phase angle degrees. This increment also reveals the complete release of the intercalated secondary inhibition DDA.

As discussed in Section 3.8 (UV−vis analysis), the primary inhibitor, IM, shows effective release in both basic and acidic media and thus provides a barrier to the corrosive species at the initial stage of the scratch, while DDA working in the acidic environment enables the hybrid coatings to perform efficiently in the later stages of scratch. The corrosion inhibition of the steel substrate by IM is attributed to the adsorption of IM molecules on the negatively charged substrate. The IM molecules have three adsorption sites, including the nitrogen atom with sp^2 lone pair of electrons, the hydrogen atom attached to the nitrogen, and the π bond of the aromatic ring. It is also studied previously[54] that most of the organic compounds containing nitrogen atoms inhibit the corrosion process by electron donation from the nitrogen atom and by bridging with the active hydrogen atom attached to the N atom. On the contrary, the π bond of the aromatic ring also facilitates the adsorption of these molecules. The IM molecules adsorb parallel to steel substrate in the scratched zone, which hinders the penetration of the electrolyte and thus increases the barrier properties of the scratched steel in NaCl solution.[63] When the IM molecules are released from the HNTs, they cover most of the exposed steel surface because of better compression in them and thus provide an efficient anti-corrosive behavior to the modified and hybrid coatings compared to the reference coatings. In addition, at the initial stages of immersion, the hybrid coatings uptake the electrolyte slowly, which enables the localized pH to be more acidic and triggers the intercalated DDA to be released from the multilayers of HHNTs. The DDA, after releasing, is adsorbed on the exposed steel substrate and adds an additional layer to the protective layer formed by the adsorption of IM at the scratched area of the steel surface (Figure 14). It replaces, on average 2.32 water molecules per DDA.[64] Furthermore, there are excessive negative charges on the steel surface; therefore, the DDA molecules can efficiently adsorb on the steel surface both physically and chemically. To sum up, the inhibition mechanism of DDA for the scratched region of the coating is a geometric blocking effect for the electrolyte to penetrate the steel substrate. In summary, both the IM and DDA in the hybrid coatings provide an effective barrier against corrosion species to penetrate into the coating and hence prevent the corrosion process. These findings are consistent with the previous studies.[18,19,33,65−67]

To quantify further the inhibition effect of IM and DDA, the electrochemical parameters were calculated by using the equivalent circuits, as shown in Figure 11. The R_p of reference coatings analyzed was approximately 0.5×10^6 Ω cm^2, which

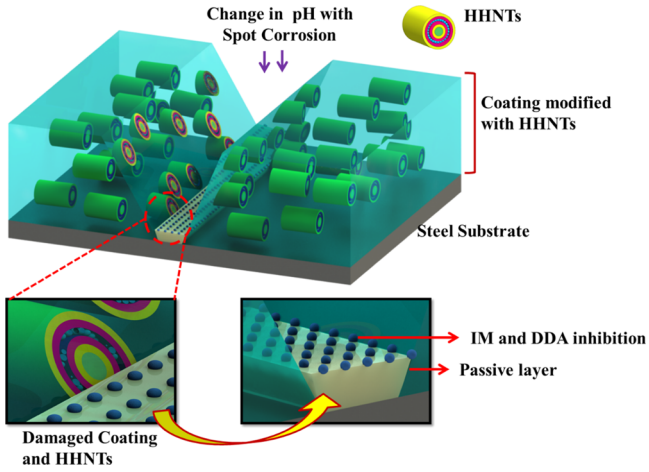

Figure 14. Protective self-healing mechanism of the hybrid coatings.

decreases continuously with the increase in immersion time and reaches to 5.5×10^5 Ω cm^2 after seven days explaining the deterioration of the reference coatings over time. On the contrary, the modified and hybrid coatings result in much stable R_p values. The R_p values of modified and hybrid coatings show an increase with increasing immersion time, reflecting the efficient barrier capability of IM and DDA in the scratched region. The calculated R_p of the modified and hybrid coatings are 4.5×10^6 and 12.2×10^6 Ω cm^2, respectively, at the initial stage of immersion, which increases to 41.7×10^6 and 252.7×10^6 Ω cm^2, respectively, after seven days of immersion. At the initial stages of the immersion of coatings, the low-frequency resistance explained the corrosive activity on the steel interface, which was almost 1×10^6 Ω cm^2 for all the reference, modified, and smart hybrid self-healing polymeric coatings. The R_{ct} of the reference coatings shows a slight decrease over the immersion period. At the end of the test, the reference coating decreased by one order, showing a R_{ct} value of 1×10^5 Ω cm^2 On the contrary, the modified and hybrid coatings show an increase of R_{ct} value. After the seventh day of immersion, the R_{ct} value of modified and hybrid coatings increased by two and three orders, respectively. This increase in the magnitude of R_{ct} in modified and hybrid coatings confirms the negligible corrosion activity on the steel surface. Moreover, the improvement in R_{ct} is also consistent with the increase in R_p for the modified and hybrid coatings. The R_p and R_{ct} values of the scratched coatings over the emersion period are depicted in Figure 15.

To confirm the release of the corrosion inhibitors, SEM/EDX analysis of the scratched areas of the developed coatings after the immersion in 3.5 wt % NaCl solution for 72 h was investigated, depicted in Figure 16. From the SEM analysis (Figure 10a,c,e), it is observed that there is a dominant passive layer formed in modified and hybrid coatings compared with the reference coatings. Furthermore, Al and Si are detected by EDX spectra (Figure 10b,d,f), which confirms the presence of HNTs in the develop coatings. Chlorides were also found in the scratched area, as expected after exposure to NaCl solution. The drastic change in the peak intensities of the carbon in the modified and hybrid coating confirms the presence of organic inhibitors in the scratched area.[68] The carbon intensity further increased in the hybrid coating because of the long-chain aliphatic structure of DDA. The results are in line with high corrosion impeding abilities of these coatings shown in EIS analysis and maximum

https://dx.doi.org/10.1021/acsami.0c08953
ACS Appl. Mater. Interfaces 2020, 12, 37571−37584

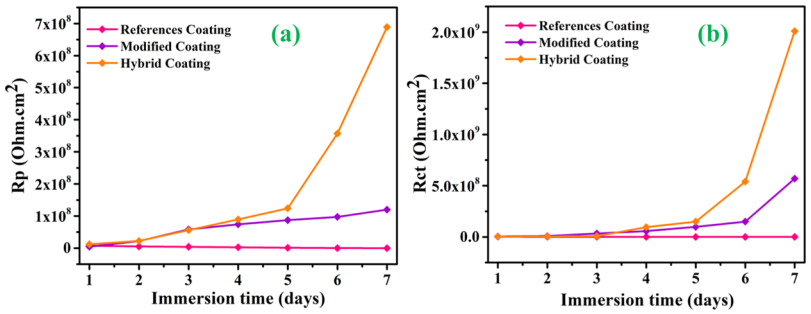

Figure 15. Variation of electrochemical parameters with immersion time; (a) charge transfer resistance of coatings and (b) pore resistance of the coatings.

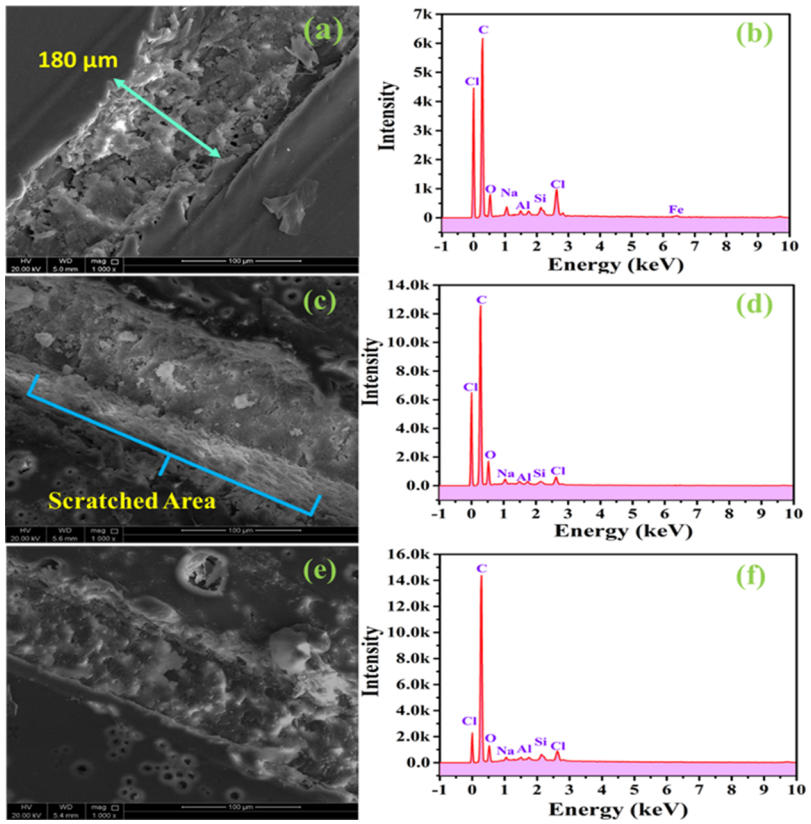

Figure 16. FE-SEM and EDX of the developed coatings after immersion in 3.5 wt % NaCl solution for 72 h; (a,b) reference coating, (c,d) modified coatings, and (e,f) hybrid coatings.

release of the inhibitor in the UV analysis after 72 h of immersion.

The photographs of scratched developed coatings (Figure 17) depict that the reference coating, which is doped with as-received HNTs, is unable to protect the steel substrate from the corrosion process efficiently. Hence, extensive corrosion initiation signs are noticed after the seventh day of immersion in 3.5 wt % NaCl solution. Furthermore, in the case of modified coating, the IM release hinders the corrosion process from happening in the initial days, but the coatings show slight deterioration with the increasing immersion days. On the seventh day, clear corrosion initiation signs are noticed at the scratched area. On the other hand, no visible degree of corrosion was seen after analyzing hybrid scratched coating immersed for seven days. This high corrosion protection performance is mainly due to the synergetic effect of both the organic inhibitors loaded in hybrid HNTs. The efficient release over the pH range enables hybrid coatings to provide enough barrier for the penetration of corrosive and aggressive species.

4. CONCLUSIONS

Novel HHNTs were developed by utilizing the layer by layer technique. During the formation of HHNTs, IM (5 wt %) was successfully encapsulated into the lumen of HNTs, while DDA (0.4 wt %) was effectively intercalated into the polyelectrolyte layers. HHNTs were used as green smart carriers (3 wt %) in polymeric coatings for corrosion protection of steel. A comparison of the structural, thermal, mechanical, and anticorrosive properties elucidates that the hybrid coatings demonstrate superior properties compared to the reference and modified coatings. The calculated corrosion inhibition efficiencies of the modified and hybrid coatings are 92 and 99.8%, respectively, when compared to the reference coatings. The superior anticorrosion properties of the hybrid coatings can be

https://dx.doi.org/10.1021/acsami.0c08953
ACS Appl. Mater. Interfaces 2020, 12, 37571−37584

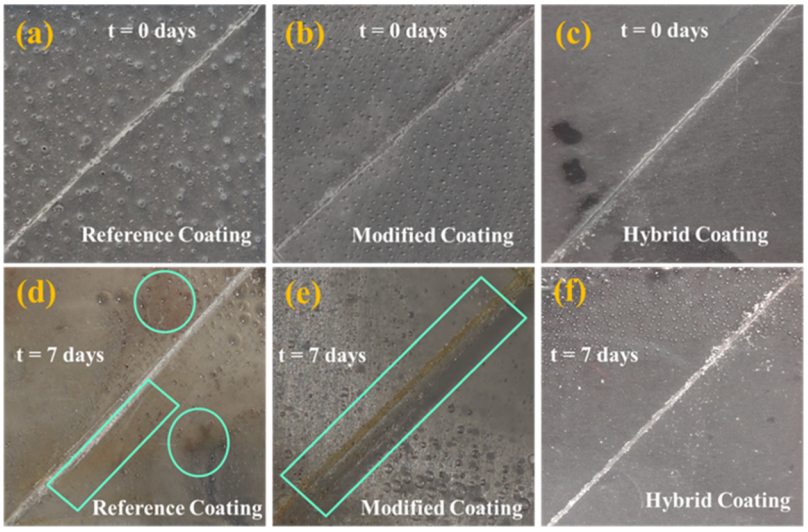

Figure 17. Photographs of scratched: reference, modified, and hybrid coatings, (a–c) before immersion and (d–f) after immersion in 3.5 wt % NaCl solution for seven days.

attributed to the synergetic effect of both the inhibitors loaded into HHNTs and their efficient release in response to the localized pH change of the corrosive medium. Moreover, an active release of IM is observed in both acidic and basic media enabling it to inhibit corrosion at the early stages of damage, while DDA being efficiently released in the acidic medium may contribute to impeding the corrosion activity at the later stages of deterioration. The improved anticorrosion properties of hybrid coatings justify the beneficial role of the development of novel HHNT nanotubes for corrosion protection. The tempting properties of hybrid coatings make them attractive for corrosion protection of steel in the oil and gas industry.

AUTHOR INFORMATION

Corresponding Author

R. A. Shakoor – *Center for Advanced Materials (CAM), Qatar University, 2713 Doha, Qatar;* orcid.org/0000-0003-3397-5309; Phone: +974-44036867; Email: Shakoorshakoor@qu.edu.qa

Authors

Adnan Khan – *Center for Advanced Materials (CAM), Qatar University, 2713 Doha, Qatar*

Amani Hassanein – *Center for Advanced Materials (CAM), Qatar University, 2713 Doha, Qatar*

Sehrish Habib – *Center for Advanced Materials (CAM), Qatar University, 2713 Doha, Qatar*

Muddasir Nawaz – *Center for Advanced Materials (CAM), Qatar University, 2713 Doha, Qatar*

Ramazan Kahraman – *Department of Chemical Engineering, Qatar University, 2713 Doha, Qatar*

Complete contact information is available at: https://pubs.acs.org/10.1021/acsami.0c08953

Notes

The authors declare no competing financial interest.

ACKNOWLEDGMENTS

This publication was made possible by NPRP11S-1226-170132 from Qatar National Research Fund (a member of the Qatar Foundation). Statements made herein are solely the responsibility of the authors. The authors would like to thank the Central laboratory Unit (CLU), Qatar University, for SEM analysis. The authors also acknowledge the support of Core lab-QEERI (HBKU) for proving TEM analysis.

REFERENCES

(1) Cozzarini, L.; Marsich, L.; Schmid, C. Ant-Nest Corrosion Failure of Heat Exchangers Copper Pipes. *Eng. Failure Anal.* **2020**, *109*, 104387.

(2) Xue, S.; Shen, R.; Chen, W.; Miao, R. Corrosion Fatigue Failure Analysis and Service Life Prediction of High Strength Steel Wire. *Eng. Failure Anal.* **2020**, *110*, 104440.

(3) Revie, R. W. *Corrosion and Corrosion Control: An Introduction To Corrosion Science And Engineering*, 4th ed.; John Wiley & Sons, 2008.

(4) Olajire, A. A. Recent Advances on Organic Coating System Technologies for Corrosion Protection of Offshore Metallic Structures. *J. Mol. Liq.* **2018**, *269*, 572–606.

(5) Erdoğdu, Ş.; Bremner, T. W.; Kondratova, I. L. Accelerated Testing of Plain and Epoxy-Coated Reinforcement in Simulated Seawater and Chloride Solutions. *Cem. Concr. Res.* **2001**, *31*, 861–867.

(6) Younos, T.; Lee, J. Desalination: Concept and System Components. *Corrosion and Fouling Control in Desalination Industry*; Springer Nature Switzerland, 2020; pp 3–27.

(7) Zahidah, K. A.; Kakooei, S.; Ismail, M. C.; Mohebbi, H.; Joshaghani, A. H.; Ghasemi, M.; Eng, K. K. *Smart Anticorrosive Coatings Containing Corrosion Inhibitor–Loaded Halloysite Nanotubes*; Elsevier Inc., 2019.

(8) Khan, A.; Sliem, M. H.; Arif, A.; Salih, M. A.; Shakoor, R. A.; Montemor, M. F.; Kahraman, R.; Mansour, S.; Abdullah, A. M.; Hasan, A. Designing and Performance Evaluation of Polyelectrolyte Multilayered Composite Smart Coatings. *Prog. Org. Coat.* **2019**, *137*, 105319.

(9) Bagale, U. B.; Sonawane, S. H.; Bhanvase, B.; Hakke, V. S.; Kakunuri, M.; Manickam, S.; Sonawane, S. S. *Multifunctional Coatings Based on Smart Nanocontainers*; Elsevier Inc., 2020.

(10) Montemor, M. F. Surface & Coatings Technology Functional and Smart Coatings for Corrosion Protection: A Review of Recent Advances. *Surf. Coat. Technol.* **2014**, *258*, 17–37.

(11) Montemor, M. F.; Vicente, C.; Técnico, I. S. *Functional Self-Healing Coatings: A New Trend in Corrosion Protection by Organic Coatings*; Elsevier, 2018.

(12) Tang, L.; Whalen, J.; Schutte, G.; Weder, C. Stimuli-Responsive Epoxy Coatings. *ACS Appl. Mater. Interfaces* **2009**, *1*, 688–696.

(13) He, Y.; Xu, W.; Tang, R.; Zhang, C.; Yang, Q. PH-Responsive Nanovalves Based on Encapsulated Halloysite for the Controlled Release of a Corrosion Inhibitor in Epoxy Coating. *RSC Adv.* **2015**, *5*, 90609–90620.

(14) Harb, S. V.; Trentin, A.; de Souza, T. A. C.; Magnani, M.; Pulcinelli, S. H.; Santilli, C. V.; Hammer, P. Effective Corrosion Protection by Eco-Friendly Self-Healing PMMA-Cerium Oxide Coatings. *Chem. Eng. J.* **2020**, *383*, 123219.
(15) Behzadnasab, M.; Mirabedini, S. M.; Kabiri, K.; Jamali, S. Corrosion Performance of Epoxy Coatings Containing Silane Treated ZrO2 Nanoparticles on Mild Steel in 3.5% NaCl Solution. *Corros. Sci.* **2011**, *53*, 89−98.
(16) Ashrafi-shahri, S. M.; Ravari, F.; Seifzadeh, D. Progress in Organic Coatings Smart Organic / Inorganic Sol-Gel Nanocomposite Containing Functionalized Mesoporous Silica for Corrosion Protection. *Prog. Org. Coat.* **2019**, *133*, 44−54.
(17) Zhao, Y.; Xu, J.-B.; Zhan, J.; Chen, Y.-Q.; Hu, J.-M. Electrodeposited Superhydrophobic Mesoporous Silica Films Co-Embedded with Template and Corrosion Inhibitor for Active Corrosion Protection. *Appl. Surf. Sci.* **2020**, *508*, 145242.
(18) Asadi, N.; Naderi, R.; Mahdavian, M. Halloysite Nanotubes Loaded with Imidazole Dicarboxylic Acid to Enhance Protection Properties of a Polymer Coating. *Prog. Org. Coat.* **2019**, *127*, 375−384.
(19) Njoku, D. I.; Cui, M.; Xiao, H.; Shang, B.; Li, Y. Understanding the Anticorrosive Protective Mechanisms of Modified Epoxy Coatings with Improved Barrier, Active and Self-Healing Functionalities: EIS and Spectroscopic Techniques. *Sci. Rep.* **2017**, *7*, 15597.
(20) Lvov, Y.; Abdullayev, E. Functional Polymer-Clay Nanotube Composites with Sustained Release of Chemical Agents. *Prog. Polym. Sci.* **2013**, *38*, 1690−1719.
(21) Joshi, A.; Abdullayev, E.; Vasiliev, A.; Volkova, O.; Lvov, Y. Interfacial Modification of Clay Nanotubes for the Sustained Release of Corrosion Inhibitors. *Langmuir* **2013**, *29*, 7439−7448.
(22) Ubaid, F.; Radwan, A. B.; Naeem, N.; Shakoor, R. A.; Ahmad, Z.; Montemor, M. F.; Kahraman, R.; Abdullah, A. M.; Soliman, A. Multifunctional Self-Healing Polymeric Nanocomposite Coatings for Corrosion Inhibition of Steel. *Prog. Org. Coat.* **2019**, *372*, 121−133.
(23) Nawaz, M.; Yusuf, N.; Habib, S.; Shakoor, R. A.; Ubaid, F.; Ahmad, Z.; Kahraman, R.; Mansour, S.; Gao, W. Development and Properties of Polymeric Nanocomposite Coatings. *Polymers* **2019**, *11*, 852.
(24) Raj, R.; Morozov, Y.; Calado, L. M.; Taryba, M. G.; Kahraman, R.; Shakoor, A.; Montemor, M. F. Inhibitor Loaded Calcium Carbonate Microparticles for Corrosion Protection of Epoxy-Coated Carbon Steel. *Electrochim. Acta* **2019**, *319*, 801−812.
(25) Raja, P. B.; Ismail, M.; Ghoreishiamiri, S.; Mirza, J.; Ismail, M. C.; Kakooei, S.; Rahim, A. A. Reviews on Corrosion Inhibitors: A Short View. *Chem. Eng. Commun.* **2016**, *203*, 1145−1156.
(26) Zahidah, K. A.; Kakooei, S.; Ismail, M. C.; Bothi Raja, P. Halloysite Nanotubes as Nanocontainer for Smart Coating Application: A Review. *Prog. Org. Coat.* **2017**, *111*, 175−185.
(27) Abdullayev, E.; Lvov, Y. Halloysite Clay Nanotubes for Controlled Release of Protective Agents. *J. Nanosci. Nanotechnol.* **2011**, *11*, 10007−10026.
(28) Liu, M.; Jia, Z.; Jia, D.; Zhou, C. Recent Advance in Research on Halloysite Nanotubes-Polymer Nanocomposite. *Prog. Polym. Sci.* **2014**, *39*, 1498−1525.
(29) Hoseinzadeh, A. R.; Javadpour, S. Investigation of Loaded Halloysite Nanotubes with Novel Inhibitor as a Smart Anticorrosion Epoxy Coating. *Mater. Res. Express* **2019**, *6*, 115703.
(30) Zeng, S.; Reyes, C.; Liu, J.; Rodgers, P. A.; Wentworth, S. H.; Sun, L. Facile Hydroxylation of Halloysite Nanotubes for Epoxy Nanocomposite Applications. *Polymer* **2014**, *55*, 6519−6528.
(31) Akbari, V.; Najafi, F.; Vahabi, H.; Jouyandeh, M.; Badawi, M.; Morisset, S.; Ganjali, M. R.; Saeb, M. R. Surface Chemistry of Halloysite Nanotubes Controls the Curability of Low Filled Epoxy Nanocomposites. *Prog. Org. Coat.* **2019**, *135*, 555−564.
(32) Saif, M. J.; Asif, H. M.; Naveed, M. Properties and Modification Methods of Halloysite Nanotubes: A State-of-The-Art Review. *J. Chil. Chem. Soc.* **2018**, *63*, 4109−4125.
(33) Xu, H.-Y.; Li, B.; Han, X.; Wang, Y.; Zhang, X.-R.; Komarneni, S. Synergic Enhancement of the Anticorrosion Properties of an Epoxy Coating by Compositing with Both Graphene and Halloysite Nanotubes. *J. Appl. Polym. Sci.* **2019**, *136*, 47562.
(34) Carneiro, J.; Caetano, A. F.; Kuznetsova, A.; Maia, F.; Salak, A. N.; Tedim, J.; Scharnagl, N.; Zheludkevich, M. L.; Ferreira, M. G. S. Polyelectrolyte-Modified Layered Double Hydroxide Nanocontainers as Vehicles for Combined Inhibitors. *RSC Adv.* **2015**, *5*, 39916−39929.
(35) Dong, C.; Zhang, M.; Xiang, T.; Yang, L.; Chan, W.; Li, C. Novel Self-Healing Anticorrosion Coating Based on L-Valine and MBT-Loaded Halloysite Nanotubes. *J. Mater. Sci.* **2018**, *53*, 7793−7808.
(36) Izadi, M.; Shahrabi, T.; Mohammadi, I.; Ramezanzadeh, B.; Fateh, A. The Electrochemical Behavior of Nanocomposite Organic Coating Based on Clay Nanotubes Filled with Green Corrosion Inhibitor through a Vacuum-Assisted Procedure. *Composites, Part B* **2019**, *171*, 96−110.
(37) Chen, C.; Xiao, G.; He, Y.; Zhong, F.; Li, H.; Wu, Y.; Chen, J. Bio-Inspired Superior Barrier Self-Healing Coating: Self-Assemble of Graphene Oxide and Polydopamine-Coated Halloysite Nanotubes for Enhancing Corrosion Resistance of Waterborne Epoxy Coating. *Prog. Org. Coat.* **2020**, *139*, 105402.
(38) Xing, X.; Wang, J.; Li, Q.; Hu, W.; Yuan, J. A Novel Acid-Responsive HNTs-Based Corrosion Inhibitor for Protection of Carbon Steel. *Colloids Surf., A* **2018**, *553*, 295−304.
(39) Ramasamy, R. Vibrational Spectroscopic Studies of Imidazole. *Arm. J. Phys.* **2015**, *8*, 51−55.
(40) Khan, A.; Ubaid, F.; Fayyad, E. M.; Ahmad, Z.; Shakoor, R. A.; Montemor, M. F.; Kahraman, R.; Mansour, S.; Hassan, M. K.; Hasan, A.; Abdullah, A. M. Synthesis and Properties of Polyelectrolyte Multilayered Microcapsules Reinforced Smart Coatings. *J. Mater. Sci.* **2019**, *54*, 12079−12094.
(41) Wu, X.; Liu, C.; Qi, H.; Zhang, X.; Dai, J.; Zhang, Q.; Zhang, L.; Wu, Y.; Peng, X. Synthesis and Adsorption Properties of Halloysite/Carbon Nanocomposites and Halloysite-Derived Carbon Nanotubes. *Appl. Clay Sci.* **2016**, *119*, 284−293.
(42) Abdullayev, E.; Price, R.; Shchukin, D.; Lvov, Y. Halloysite Tubes as Nanocontainers for Anticorrosion Coating with Benzotriazole. *ACS Appl. Mater. Interfaces* **2009**, *1*, 1437−1443.
(43) Manasa, S.; Jyothirmayi, A.; Siva, T.; Sathiyanarayanan, S.; Gobi, K. V.; Subasri, R. Effect of Inhibitor Loading into Nanocontainer Additives of Self-Healing Corrosion Protection Coatings on Aluminum Alloy A356.0. *J. Alloys Compd.* **2017**, *726*, 969−977.
(44) Lun, H.; Ouyang, J.; Yang, H. Natural Halloysite Nanotubes Modified as an Aspirin Carrier. *RSC Adv.* **2014**, *4*, 44197−44202.
(45) Lvov, Y.; Wang, W.; Zhang, L.; Fakhrullin, R. Halloysite Clay Nanotubes for Loading and Sustained Release of Functional Compounds. *Adv. Mater.* **2016**, *28*, 1227−1250.
(46) Abdullayev, E.; Shchukin, D.; Lvov, Y. Halloysite Clay Nanotubes as a Reservoir for Corrosion Inhibitors and Template for Layer-by-Layer Encapsulation. *Polym. Mater. Sci. Eng.* **2008**, *99*, 331−332.
(47) Veerabadran, N. G.; Mongayt, D.; Torchilin, V.; Price, R. R.; Lvov, Y. M. Organized Shells on Clay Nanotubes for Controlled Release of Macromolecules. *Macromol. Rapid Commun.* **2009**, *30*, 99−103.
(48) Wang, P.; Du, M.; Zhang, M.; Zhu, H.; Bao, S.; Zou, M.; Yang, T. Facile Fabrication of AuNPs/PANI/HNTs Nanostructures for High-Performance Electrochemical Sensors towards Hydrogen Peroxide. *Chem. Eng. J.* **2014**, *248*, 307−314.
(49) Ghebaur, A.; Garea, S. A.; Iovu, H. New Polymer-Halloysite Hybrid Materials - Potential Controlled Drug Release System. *Int. J. Pharm.* **2012**, *436*, 568−573.
(50) Mata, N.; Cotting, F.; Cavallaro, S.; Ochoa, N.; Aoki, I. Influence of the Chemical Treatment of Halloysite Clay in Its Loading/Release of Dodecylamine Corrosion Inhibitor to Obtain Self-Healing Coatings. *Proceedings of European Corrosion Congress EUROCORR*, 2018; Vol. *1*−*17*.
(51) Falcón, J. M.; Sawczen, T.; Aoki, I. V. Dodecylamine-Loaded Halloysite Nanocontainers for Active Anticorrosion Coatings. *Front. Mater.* **2015**, *2*, 69.

https://dx.doi.org/10.1021/acsami.0c08953
ACS Appl. Mater. Interfaces 2020, 12, 37571−37584

(52) Asadi, N.; Naderi, R.; Mahdavian, M. Progress in Organic Coatings Halloysite Nanotubes Loaded with Imidazole Dicarboxylic Acid to Enhance Protection Properties of a Polymer Coating. *Prog. Org. Coat.* **2019**, *127*, 375−384.
(53) Akbari, V.; Najafi, F.; Vahabi, H.; Jouyandeh, M.; Badawi, M.; Morisset, S.; Ganjali, M. R.; Saeb, M. R. Surface Chemistry of Halloysite Nanotubes Controls the Curability of Low Fi Lled Epoxy Nanocomposites. *Prog. Org. Coat.* **2019**, *135*, 555−564.
(54) Abdallah, M.; Megahed, H. E.; Sobhi, M. Ni2+ Cation and Imidazole as Corrosion Inhibitors for Carbon Steel in Sulfuric Acid Solutions. *Monat. Chem.* **2010**, *141*, 1287−1295.
(55) Peral, F.; Gallego, E. Self-Association of Imidazole and Its Methyl Derivatives in Aqueous Solution. A Study by Ultraviolet Spectroscopy. *J. Mol. Struct.* **1997**, *415*, 187−196.
(56) Mecheri, B.; D'Epifanio, A.; Traversa, E.; Licoccia, S. Sulfonated Polyether Ether Ketone and Hydrated Tin Oxide Proton Conducting Composites for Direct Methanol Fuel Cell Applications. *J. Power Sources* **2008**, *178*, 554−560.
(57) G, R.; G, R.; N, S.; R, C.; Hashmi, M. A. Enhancement of Mechanical Properties of Epoxy/Halloysite Nanotube (HNT) Nanocomposites. *SN Appl. Sci.* **2019**, *1*, 296.
(58) Saif, M. J.; Naveed, M.; Zia, K. M.; Asif, M. Pristine and γ-Irradiated Halloysite Reinforced Epoxy Nanocomposites - Insight Study. *Radiat. Phys. Chem.* **2016**, *127*, 115−121.
(59) Ye, Y.; Chen, H.; Wu, J.; Ye, L. High Impact Strength Epoxy Nanocomposites with Natural Nanotubes. *Polymer* **2007**, *48*, 6426−6433.
(60) Liu, M.; Guo, B.; Du, M.; Cai, X.; Jia, D. Properties of Halloysite Nanotube-Epoxy Resin Hybrids and the Interfacial Reactions in the Systems. *Nanotechnology* **2007**, *18*, 455703.
(61) Asadi, N.; Naderi, R.; Mahdavian, M. Doping of Zinc Cations in Chemically Modified Halloysite Nanotubes to Improve Protection Function of an Epoxy Ester Coating. *Corros. Sci.* **2019**, *151*, 69−80.
(62) Raj, R.; Morozov, Y.; Calado, L. M.; Taryba, M. G.; Kahraman, R.; Shakoor, R. A.; Montemor, M. F. Calcium Carbonate Particles Loaded with Triethanolamine and Polyethylenimine for Enhanced Corrosion Protection of Epoxy Coated Steel. *Corros. Sci.* **2020**, *167*, 108548.
(63) Gutiérrez, E.; Rodríguez, J. A.; Cruz-Borbolla, J.; Alvarado-Rodríguez, J. G.; Thangarasu, P. Development of a Predictive Model for Corrosion Inhibition of Carbon Steel by Imidazole and Benzimidazole Derivatives. *Corros. Sci.* **2016**, *108*, 23−35.
(64) Chen, Z.; Huang, L.; Qiu, Y.; Guo, X. Inhibition Effect of Dodecylamine on Carbon Steel Corrosion in Hydrochloric Acid Solution. *Surf. Rev. Lett.* **2012**, *19*, 1250060.
(65) Huttunen-Saarivirta, E.; Vaganov, G. V.; Yudin, V. E.; Vuorinen, J. Characterization and Corrosion Protection Properties of Epoxy Powder Coatings Containing Nanoclays. *Prog. Org. Coat.* **2013**, *76*, 757−767.
(66) Jia, Y.; Qiu, T.; Guo, L.; Ye, J.; He, L.; Li, X. Preparation of PH Responsive Smart Nanocontainer via Inclusion of Inhibitor in Graphene/Halloysite Nanotubes and Its Application in Intelligent Anticorrosion Protection. *Appl. Surf. Sci.* **2020**, *504*, 144496.
(67) Wang, M.; Wang, J.; Hu, W. Preparation and Corrosion Behavior of Cu-8-HQ@HNTs/Epoxy Coating. *Prog. Org. Coat.* **2020**, *139*, 105434.
(68) Amin, M. A.; Abd El-Rehim, S. S.; El-Sherbini, E. E. F.; Bayoumi, R. S. The Inhibition of Low Carbon Steel Corrosion in Hydrochloric Acid Solutions by Succinic Acid. Part I. Weight Loss, Polarization, EIS, PZC, EDX and SEM Studies. *Electrochim. Acta* **2007**, *52*, 3588−3600.

https://dx.doi.org/10.1021/acsami.0c08953
ACS Appl. Mater. Interfaces 2020, 12, 37571−37584